Geometric Calibration of a New Miniaturized Endoscopic Ultrasound Probe

João Cavalcanti Santos, Lucas Lavenir, Nabil Zemiti, Philippe Poignet, Frederic Venail

Geometric Calibration of a New Miniaturized Endoscopic Ultrasound Probe

João Cavalcanti Santos[1], Lucas Lavenir[2], Nabil Zemiti[2], Philippe Poignet[2] and Frederic Venail[1]

***Abstract*— The present paper proposes a method for the geometric calibration of a new endoscopic ultrasound (US) probe designed for the imaging of the inner ear. Such US probe has 24 elements and a distal diameter equal to 4 mm. The atypical probe miniaturized geometry may raise doubts about the applicability of existing state-of-the-art calibration methods. This work answers such question. The results presented in this paper indicate that the proposed straightforward calibration procedure leads to satisfying accuracy. The phantom used for the geometric calibration have wires as reference geometry and its dimensions are taken based on a microtomography acquisition. The obtained results may enable the US image-guided navigation of the human inner ear.**

I. Introduction

Ultrasound (US) presents several well-known advantages in comparison to other medical imaging modalities, *e.g.* easy intraoperative application, reduced cost and acquisition time, portability and tolerability [1], [2]. Nevertheless, when compared to typical imaging modalities such as computed tomography (CT) and magnetic resonance imaging (MRI), US imaging presents inferior image quality. Furthermore, the acquisition of large anatomical volumes using ultrasonography leads to additional technical problems [3]. Performing an automatized displacement of a US probe while keeping acoustic coupling is usually a challenging task [4]. In an effort to overcome these drawbacks while keeping the aforementioned advantages, special attention has been devoted to the improvement of 3D US imaging. Examples of subjects notably addressed in this context are calibration of US probes [5], registration [6] and 3D reconstruction [7].

The present paper addresses the geometric calibration of a US endoscopic probe designed for the imaging of the inner ear. The geometric calibration of a US probe aims at finding the rigid transformation relating the pose of a tracking device attached to the probe holder and the coordinate system of the US images. Knowing such transformation in addition to the global position of the tracking device, each pixel of the US image can be related to a point in the global coordinate system. This information is particularly useful for the so-called freehand 3D US imaging [8] and for the intraoperative navigation [9]. The tracked and unconstrained motion of the US probe can lead to the acquisition of complex and large anatomical volumes. In this case, the US acquisition should go along with a temporal calibration of the tracked position of the probe holder. On the other hand, if a motorized probe holder is used, a 3D volume can be reconstructed with a constant pose of the tracking device, as in [10]. This is the case depicted in Figure 1 and studied in this paper. 3D US volumes are acquired using scan-conversion (*e.g.* [11]) based on a collection of 2D images taken with different values of θ (as shown in Figure 1).

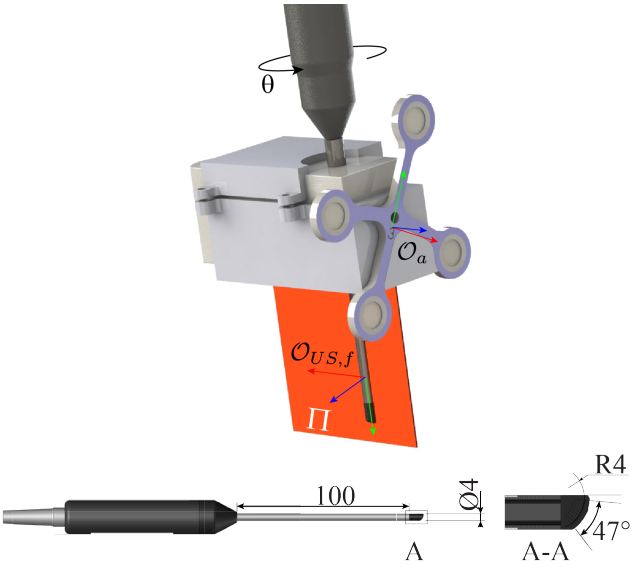

Fig. 1. CAD view of the US probe mounted on a robotic arm and main dimensions of the miniaturized probe. The pose of the robotic arm is tracked by means of a reflective marker.

Several methods for the geometric calibration of US probes have been proposed in the state-of-the-art. Typically, the calibration is performed by means of the acquisition of a phantom with known geometry and physical properties. Commonly used phantoms present reference geometries that approximate single-points [12], straight lines [13] and planes [14]. Furthermore, both linear [3] and convex [15] probes were addressed.

The present paper details a method for the calibration of the probe depicted in Figure 1. Albeit the modest novelty involved in the rather straightforward proposed calibration procedure, the contribution of this paper relies in the unusual small dimensions of the calibrated probe, as depicted in Figure 1. This convex endoscopic miniaturized probe has acoustic elevation focus of 8 mm, central frequency 18MHz and distal diameter of 4 mm. This probe presents, above all, an uncommon small number of elements, namely 24.

[1] João Cavalcanti Santos and Frederic Venail are with INM, Univ. Montpellier, INSERM, Montpellier, France, joao.cavalcanti-santos@inserm.fr, f-venail@chu-montpellier.fr

[2]Lucas Lavenir, Nabil Zemiti and Philippe Poignet are with LIRMM, Univ. Montpellier, CNRS, Montpellier, France, {lavenir, zemiti, poignet}@lirmm.fr

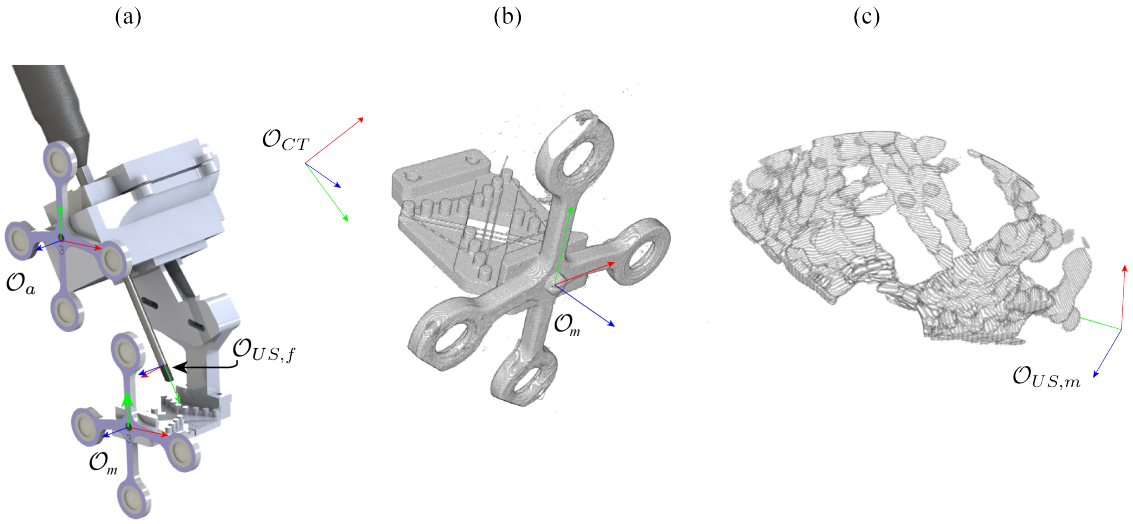

Fig. 2. (a) Complete CAD view of the assembly used in the calibration, (b) CT volume of the calibration phantom (c) US reconstructed volume of the phantom reference geometry.

The elements are positioned with a constant pitch of 0.1 mm. Most of the previous studies addressing the geometric calibration of US probes consider transducers with more than 128 elements (see, for instance [6], [8], [10], [16]–[18]). Accordingly, the question of whether common calibration methods could lead to satisfying results with the aforementioned atypical characteristics represents a relevant inquiry.

The calibration is performed using a tracked phantom, which presents a set of wires as reference geometry. The wire poses are handled as straight line segments. A precise measure of the phantom geometry is obtained through high resolution micro-tomography.

The present paper is organized as follows. Section II introduces the main goal of the proposed calibration and the used materials. Section III discusses the overall rationale applied during the geometric calibration. Details on the image processing of the reference phantom are presented in Section IV. Using the results of such processing, the rigid transformation corresponding to the probe calibration is obtained in Section V. A validation procedure is detailed in Section VI and conclusions are drawn in Section VIII.

II. Preliminaries

The present paper proposes a calibration procedure for the US miniaturized probe (depicted in Figure 1) mounted on a robotic arm. A CAD view of the used assembly is presented in Figure 1. The robotic arm is responsible for the angular positioning of θ (in accordance with Figure 1) during a 3D volume acquisition. This figure also introduces two Coordinate Systems (CS): $\mathcal{O}_a$ and $\mathcal{O}_{US,f}$. The CS $\mathcal{O}_a$ corresponds to a marker rigidly fixed to the robotic arm. The y axis of $\mathcal{O}_{US,f}$ is co-linear to the US probe axis of rotation and its x axis is coincident to the symmetry plane Π of the robotic arm, as illustrated in Figure 1.

Note that $\mathcal{O}_{US,f}$ is attached to the robotic arm, and not to the US probe. Indeed, the f subscript of this CS stands for *fixed* considering a 3D acquisition on which the robotic arm remains fixed and the US probe rotates around the y axis of $\mathcal{O}_{US,f}$. The calibration described in this paper aims at the estimation of the constant rigid transformation $\mathbf{T}^a_{US,f}$ between $\mathcal{O}_a$ and $\mathcal{O}_{US,f}$.

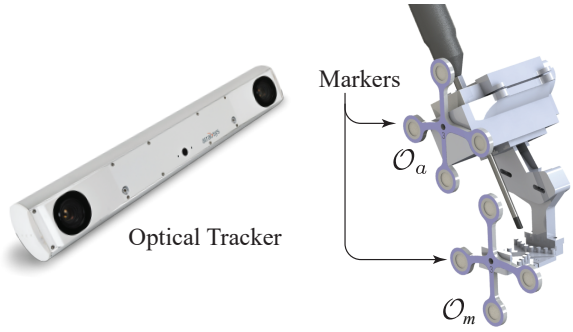

Fig. 3. Overall set-up used for the calibration of the US probe.

The pose of $\mathcal{O}_a$ in the global coordinate system is given thanks to the pose measurement of the corresponding marker. More in detail, an optical tracker Atracsys fusionTrack 500 is used to measure the positions of each of the reflective fiducials, which leads to the estimation of the pose of $\mathcal{O}_a$. This optical tracking systems presents a typical fiducial localization error of 0.08 mm, which is consistent with the expected precision for the US probe calibration.

For known pose of $\mathcal{O}_a$, transformation $\mathbf{T}^a_{US,f}$ and angle θ, each pixel of the corresponding US image can be correlated to a point positioned with respect to the global coordinate system. The overall set-up is depicted in Figure 3.

III. Overall Calibration Procedure

The estimation of $\mathbf{T}^a_{US,f}$ is based on US acquisitions of a position tracked phantom with well known geometry. A μCT volume of the phantom is used in order to obtain a

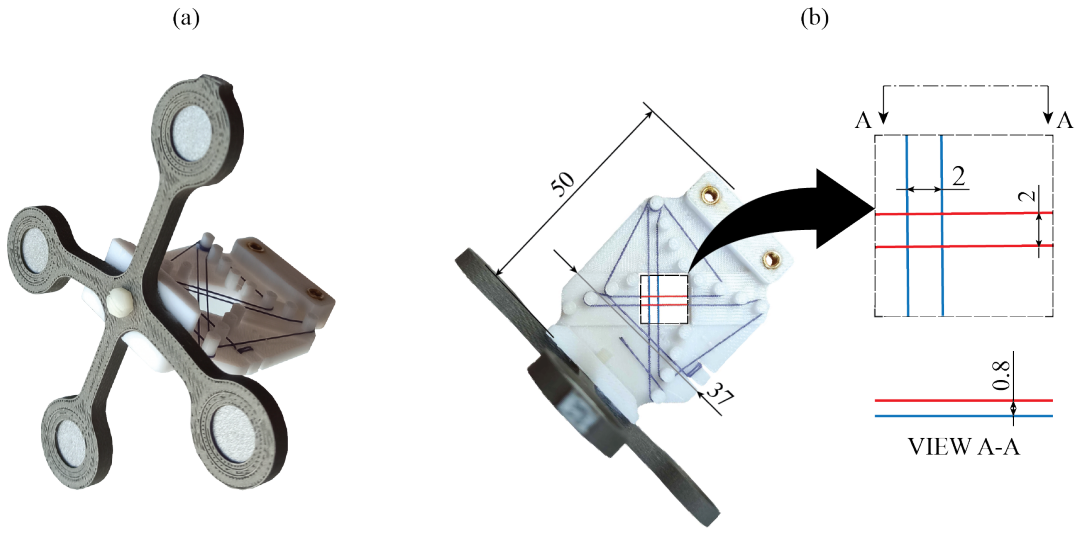

Fig. 4. Calibration phantom - (a) isometric view and (b) top view with main dimensions of the plastic structure and wires.

precise measurement of the geometry of this part. Figure 2 illustrates the complete set of CSs involved in the calibration procedure and the corresponding assembly. $\mathcal{O}_{CT}$ denotes the CS of a CT image of the phantom and, similarly, $\mathcal{O}_{US,m}$ corresponds to a US volume. In accordance with the state-of-the-art [5], [19], reference geometries using wires lead to US acquisitions with relatively good quality. More precisely, the wires lead to reduced distortion due to acoustic phenomena and they can be easily segmented from the US volume. For these reasons, the phantom presents as reference geometry a set of wires representing approximations of straight line segments. These reference geometries should be recognized in both CT and US acquisitions, so that the position of the phantom wires can be written with respect to these two CSs ($\mathcal{O}_{CT}$ and $\mathcal{O}_{US,m}$).

As an example, consider a geometrical feature or a set of n points $\mathbf{p}_i$, $i = 1, ..., n$, for a given positive integer n. Clearly, these points should be positioned in the phantom wires, which are taken as the reference geometry. Such set of points can be written with respect to both $\mathcal{O}_{CT}$ and $\mathcal{O}_{US,m}$ as $\mathbf{p}_i^{CT}$ and $\mathbf{p}_i^{US,m}$, respectively. These points can be defined taking into account the CT and the 3D US acquisition. The geometric calibration of the US probe can be seen as the definition of a $\mathbf{T}_{US,f}^{a}$ that minimizes the errors

$$e_i = \left\| \mathbf{p}_i^{CT} - \mathbf{T}_m^{CT}\, \mathbf{T}_a^m\, \mathbf{T}_{US,f}^a\, \mathbf{T}_{US,m}^{US,f}\, \mathbf{p}_i^{US,m} \right\|. \quad (1)$$

As shown in Section IV, instead of a finite set of reference points used in this illustrative example, the straight line segments related to each phantom wire can be better represented using a unique reference point and a unitary direction vector.

Section IV describes how the wires of the phantom can be identified as straight line segments on the CT and 3D US acquisitions. Based on these identified straight line segments, Section V discusses how a suitable $\mathbf{T}_{US,f}^{a}$ can be computed.

Moreover, it is important to highlight that the following rigid transformations can be easily obtained:

- $\mathbf{T}_{CT}^{m}$ - The rigid transformation relating the phantom marker CS $\mathcal{O}_m$ with respect to the CT image CS is given by the identification of the fiducial positions in the CT volume;
- $\mathbf{T}_{m}^{a}$ - This transformation is obtained directly using the measurements of the poses of $\mathcal{O}_a$ and $\mathcal{O}_m$ using an optical tracker;
- $\mathbf{T}_{US,m}^{US,f}$ - The applied US reconstruction method computes the position of the origin of $\mathcal{O}_{US,f}$ with respect to $\mathcal{O}_{US,m}$ (denoted as $\mathbf{o}_{US,f}^{US,m}$). The unit vectors $\mathbf{y}_{US,m}$ and $\mathbf{y}_{US,f}$ corresponding to the y axes of $\mathcal{O}_{US,m}$ and $\mathcal{O}_{US,f}$, respectively, are parallel (*i.e.*: $\mathbf{y}_{US,f} = \mathbf{y}_{US,m}$). The relative orientation between $\mathbf{x}_{US,m}$ and $\mathbf{x}_{US,f}$ is defined in accordance to the orientations θ recorded during the US acquisition.

One may note that $\mathbf{T}_{US,f}^{a}$ is the unique unknown rigid transformation between the CSs depicted in Figure 2.

IV. Calibration Phantom Analysis

The calibration is performed using the phantom[1] depicted in Figure 4. It presents four wires that can be easily identified in a US acquisition. The wires used as reference geometry are composed of surgical suture fixed in a 3D printed structure. Additionally, the marker is used to define the relative position of the phantom with respect to the robotic arm. A high-precision 3D model of the phantom was obtained using a μCT scanner (voxel size of 65 μm, which is sufficiently precise for the expected calibration accuracy). This 3D model enables the definition of the relative position of the wires with respect to the $\mathcal{O}_m$. The calibration phantom is free of high density materials, which could deteriorate the accuracy of the CT acquisition.

The wires used as reference geometry are considered as straight line segments. Simple thresholding combined with linear regression leads to the pose of these lines in

[1]CAD model available in https://seafile.lirmm.fr/f/8e05f2f00cfc4438be4d/.

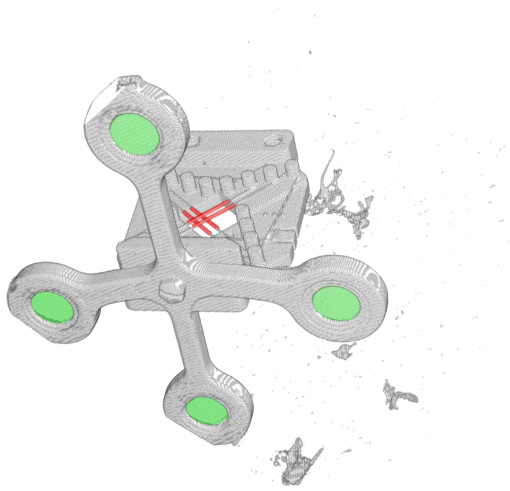

Fig. 5. Wires (red) and fiducials (green) identified in the CT volume.

the CT volume, as shown in Figure 5. Before applying linear regression, each wire is isolated from the rest of the CT volume using a manually defined cylinder. The linear regression results in a point $\mathbf{p}_{i,CT}^{CT} \in \mathbb{R}^3$ and unit vector $\mathbf{e}_{i,CT}^{CT}$ defined so that the straight line

$$\mathcal{L}_i^{CT} = \{\mathbf{p} \in \mathbb{R}^3 \mid \exists\, \lambda \in \mathbb{R},\ \mathbf{p} = \mathbf{p}_{i,CT}^{CT} + \lambda\, \mathbf{e}_{i,CT}^{CT}\} \quad (2)$$

represents each wire $i = 1, ..., 4$.

In order to represent each $\mathcal{L}_i$ in different CSs, the position of the fiducials in $\mathcal{O}_{CT}$ should be estimated. To this end, one may define the set of visible points on the region of a plane corresponding to each fiducial. The fiducial position is given by the centroid of this set of visible points. Figure 5 depicts the fiducial visible points in the acquired CT volume.

The wire poses identified in the CT acquisition should be compared to the corresponding poses in the reconstructed US volume. The identification of wire poses in the US volume applies a method similar to the one used for the CT volume, *i.e.* manual segmentation combined to linear regression. Due to the low quality of the US images, an adapted approach is necessary in order to isolate each wire from the entire US acquisition. Namely, elliptical prisms are used instead of simple cylinders. Figure 6 depicts an example of a wire segmented from the original US volume. Similarly to the wire detection applied for the CT acquisition, the linear regression of a wire in the US leads to a pair of vectors $\mathbf{p}_{i,US}^{US,m}$ and $\mathbf{e}_{i,US}^{US,m}$.

V. Computation of $\mathbf{T}_{US,f}^{a}$

Considering the rigid transformations described in Section III, the wire poses identified in the CT acquisition can be written with respect to $\mathcal{O}_a$ as

$$\begin{aligned} \overline{\mathbf{p}}_{i,CT}^{a} &= \mathbf{T}_{m}^{a}\, \mathbf{T}_{CT}^{m}\, \overline{\mathbf{p}}_{i,CT}^{CT} \\ \mathbf{e}_{i,CT}^{a} &= \mathbf{R}_{m}^{a}\, \mathbf{R}_{CT}^{m}\, \mathbf{e}_{i,CT}^{CT} \end{aligned} \quad (3)$$

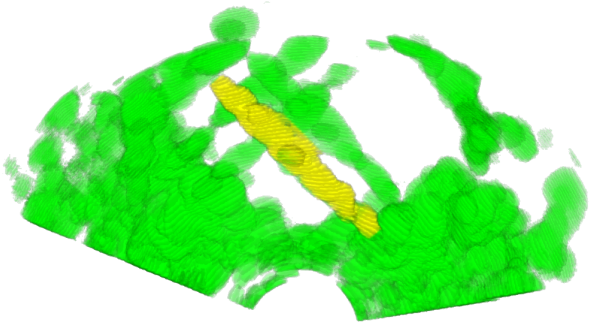

Fig. 6. An example of a wire segmented from the original US acquisition.

where $\overline{\mathbf{v}} = \begin{bmatrix}\mathbf{v}^T & 1\end{bmatrix}^T$ for any $\mathbf{v} \in \mathbb{R}^3$ and $\mathbf{R}_{c_1}^{c_2} \in \mathbb{R}^{3\times3}$ is the rotation matrix extracted from the first three rows and columns of a homogeneous matrix $\mathbf{T}_{c_1}^{c_2}$.

Similarly, the wire poses identified in the US acquisition can be written with respect to the $\mathcal{O}_{US,f}$ as

$$\begin{aligned} \overline{\mathbf{p}}_{i,US}^{US,f} &= \mathbf{T}_{US,m}^{US,f}\, \overline{\mathbf{p}}_{i,US}^{US,m} \\ \mathbf{e}_{i,US}^{US,f} &= \mathbf{R}_{US,m}^{US,f}\, \mathbf{e}_{i,US}^{US,m} \end{aligned} \quad (4)$$

The definition of $\mathbf{T}_{US,f}^{a}$ should relate the wire poses given by (3) and (4). First, the orientation of such transformation can be determined choosing a rotation matrix $\mathbf{R}_{US,f}^{a} = \mathbf{R}(\boldsymbol{\varphi}^*)$ taking as argument a vector $\boldsymbol{\varphi}^* \in \mathbb{R}^3$ of Euler angles such that

$$\boldsymbol{\varphi}^* = \arg\min_{\boldsymbol{\varphi}}\ -\mathrm{tr}\left(\mathbf{E}_{CT}^{a\,T}\, \mathbf{R}_{US,f}^{a\,T}\, \mathbf{E}_{US}^{US,f}\right), \quad (5)$$

where $\mathbf{E}_{CT}^{a} = \begin{bmatrix}\mathbf{e}_{1,CT}^{a} & \mathbf{e}_{2,CT}^{a} & \mathbf{e}_{3,CT}^{a} & \mathbf{e}_{4,CT}^{a}\end{bmatrix}$ and $\mathbf{E}_{US}^{US,f} = \begin{bmatrix}\mathbf{e}_{1,US}^{US,f} & \mathbf{e}_{2,US}^{US,f} & \mathbf{e}_{3,US}^{US,f} & \mathbf{e}_{4,US}^{US,f}\end{bmatrix}$. Note that $\boldsymbol{\varphi}^*$ obtained in (5) maximizes the sum of the inner products between $\mathbf{e}_{i,CT}^{a}$ and $\mathbf{R}_{US,f}^{a}\, \mathbf{e}_{i,US}^{US,f}$, for $i = 1, \ldots, 4$.

Finally, the translation vector $\mathbf{o}_{US,f}^{a}$ in accordance with

$$\mathbf{T}_{US,f}^{a} = \begin{bmatrix}\mathbf{R}_{US,f}^{a} & \mathbf{o}_{US,f}^{a} \\ \mathbf{0} & 1\end{bmatrix} \quad (6)$$

should be defined. To do so, one may use the projection of each pair of perpendicular straight line segments resulting in a set of eight points, such as illustrated in Figure 7. This is repeated for both (3) and (4) leading to two sets of points. Computing the centroid of these sets, $\mathbf{c}_{US}^{US,f}$ and $\mathbf{c}_{CT}^{a}$ can be related using $\mathbf{o}_{US,f}^{a} = \mathbf{c}_{CT}^{a} - \mathbf{c}_{US}^{US,f}$.

VI. Validation Procedure

In order to validate the procedure proposed in the previous sections, the calibration results were confronted with an additional US acquisition as depicted in Figure 8. The phantom was positioned with flipped orientation and opposite values of θ with respect to the ones used during the calibration. While $-160° < \theta < -20°$ during the calibration, the validation was applied for $20° < \theta < 160°$. The obtained US

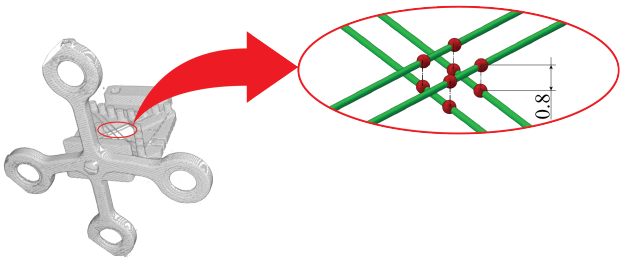

Fig. 7. The definition of $\mathbf{o}^a_{US,f}$ is based on the set of points obtained computing the projection between perpendicular straight lines (red points). Note that, in accordance with Figure 4-(b), perpendicular wires are spaced 8 mm apart vertically.

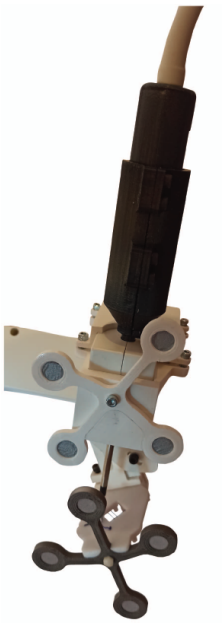

Fig. 8. Set-up disposition used to validate the calibration procedure.

Fig. 9. US volume obtained for the validation of the proposed calibration procedure.

volume was overlaid on the original CT acquisition applying

$$\mathbf{T}^{CT}_{US,m} = \mathbf{T}^{CT}_{m}\,\mathbf{T}^{m}_{a}\,\mathbf{T}^{a}_{US,f}\,\mathbf{T}^{US,f}_{US,m} = \begin{bmatrix} \mathbf{R}^{CT}_{US,m} & \mathbf{o}^{CT}_{US,m} \\ \mathbf{0} & 1 \end{bmatrix} \quad (7)$$

obtained from the calibration. The result is shown in Figure 10.

Whereas the Figure 10 indicates that an appropriate transformation $\mathbf{T}^a_{US,f}$ was obtained, this visual result does not present any quantitative evaluation related to the obtained precision. An estimation of the calibration error can be obtained registering the US acquisition of Figure 9 directly on the CT volume of Figure 4-(b). This registration, which was performed with a similar procedure as in Section V, leads to the alternative transformation

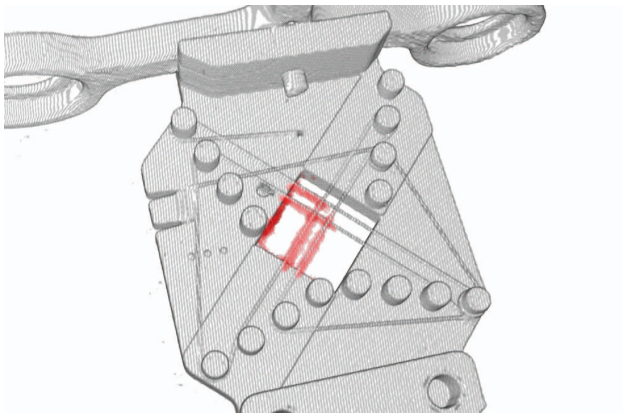

Fig. 10. US acquisition (red) overlaid on the CT volume in accordance with the calibrated transformation $\mathbf{T}^a_{US,f}$.

$$\hat{\mathbf{T}}^{CT}_{US,m} = \begin{bmatrix} \hat{\mathbf{R}}^{CT}_{US,m} & \hat{\mathbf{o}}^{CT}_{US,m} \\ \mathbf{0} & 1 \end{bmatrix}. \quad (8)$$

Although the calibration error cannot be computed due to the lack of a reliable ground truth, the divergence between $\hat{\mathbf{T}}^{CT}_{US,m}$ and $\mathbf{T}^{CT}_{US,m}$ can be seen as an estimation of this error. The translational error is given simply by $e_t = \|\mathbf{o}^a_{US,m} - \hat{\mathbf{o}}^a_{US,m}\|$. The orientational error e_o is obtained analyzing the angle related to the rotation matrix $\mathbf{R}_e = \left(\mathbf{R}^a_{US,m}\right)^T \hat{\mathbf{R}}^a_{US,m}$. Finally, the calibration errors could be estimated as $e_t = 0.49$ mm and $e_o = 1.15°$. Clearly, considering the limited experimental data addressed in the present section, these errors represent a preliminary estimation of the calibration accuracy.

Given that studies addressing the calibration of US probes frequently target submillimetric accuracy (*e.g.* [5], [19]), these are considered satisfying results. At any rate, these errors indicate that the proposed calibration procedure leads to acceptable accuracy in the context of the inner ear surgery.

VII. Acknowledgments

This work was supported in part by the Fondation Pour l'Audition (FPA RD-2017-4) and the French Occitanie Region. The authors also acknowledge the MRI platform member of the national infrastructure France-BioImaging supported by the French National Research Agency (ANR-10-INBS-04, "Investments for the future"), the labex CEMEB (ANR-10-LABX-0004) and NUMEV (ANR-10-LABX-0020).

VIII. Conclusions

The present paper introduced a rather simple calibration procedure compatible with a US endoscopic miniaturized

probe designed for the imaging of the inner ear. The obtained results indicate that proposed methodology leads to satisfactory precision. Due to the geometric constraints involved in this kind of imaging, the studied US probe presents dimensions atypically small when compared to the probes addressed in previous works proposing US geometric calibration methods. Therefore, the presented results suggest that elementary calibration approaches are also valid for miniaturized dimension probes.

Future works may apply the discussed results for image-guided navigation and address the definition of more elaborate calibration procedures (*e.g.* automatic 3D calibration). Additionally, further experiments should be performed in order to thoroughly validate the calibration procedure and extend the preliminary results discussed in the present paper. Finally, the proposed procedure can be tested in non-miniaturized US probes.

REFERENCES

[1] M. H. Mozaffari and W.-S. Lee, "Freehand 3-D Ultrasound Imaging: A Systematic Review," *Ultrasound in Medicine & Biology*, vol. 43, no. 10, pp. 2099–2124, 2017. [Online]. Available: https://www.sciencedirect.com/science/article/pii/S0301562917302776

[2] J. M. Rubin, M. Mirfakhraee, E. E. Duda, G. J. Dohrmann, and F. Brown, "Intraoperative ultrasound examination of the brain." *Radiology*, vol. 137, no. 3, pp. 831–832, 1980.

[3] F. Cenni, D. Monari, K. Desloovere, E. Aertbeliën, S.-H. Schless, and H. Bruyninckx, "The reliability and validity of a clinical 3D freehand ultrasound system," *Computer Methods and Programs in Biomedicine*, vol. 136, pp. 179–187, 2016. [Online]. Available: https://www.sciencedirect.com/science/article/pii/S0169260716304874

[4] W. . Zhu, S. E. Salcudean, S. Bachmann, and P. Abolmaesumi, "Motion/force/image control of a diagnostic ultrasound robot," in *Proceedings 2000 ICRA. Millennium Conference. IEEE International Conference on Robotics and Automation. Symposia Proceedings (Cat. No.00CH37065)*, vol. 2, 2000, pp. 1580–1585 vol.2.

[5] F. Lindseth, G. A. Tangen, T. Langø, and J. Bang, "Probe calibration for freehand 3-D ultrasound," *Ultrasound in Medicine and Biology*, vol. 29, no. 11, pp. 1607–1623, nov 2003. [Online]. Available: https://doi.org/10.1016/S0301-5629(03)01012-3

[6] C. Che, T. S. Mathai, and J. Galeotti, "Ultrasound registration: A review," *Methods*, vol. 115, pp. 128–143, 2017. [Online]. Available: https://www.sciencedirect.com/science/article/pii/S1046202316304789

[7] D. Ni, Y. P. Chui, Y. Qu, X. Yang, J. Qin, T.-T. Wong, S. S. H. Ho, and P. A. Heng, "Reconstruction of volumetric ultrasound panorama based on improved 3D SIFT," *Computerized Medical Imaging and Graphics*, vol. 33, no. 7, pp. 559–566, 2009. [Online]. Available: https://www.sciencedirect.com/science/article/pii/S0895611109000640

[8] M. I. Daoud, A. Alshalalfah, F. Awwad, and M. Al-Najar, "Freehand 3D ultrasound imaging system using electromagnetic tracking," in *2015 International Conference on Open Source Software Computing (OSSCOM)*, 2015, pp. 1–5.

[9] M. Nakamoto, K. Nakada, Y. Sato, K. Konishi, M. Hashizume, and S. Tamura, "Intraoperative Magnetic Tracker Calibration Using a Magneto-Optic Hybrid Tracker for 3-D Ultrasound-Based Navigation in Laparoscopic Surgery," *IEEE Transactions on Medical Imaging*, vol. 27, no. 2, pp. 255–270, 2008.

[10] J. Shen, N. Zemiti, J. Dillenseger, and P. Poignet, "Fast And Simple Automatic 3D Ultrasound Probe Calibration Based On 3D Printed Phantom And An Untracked Marker," in *2018 40th Annual International Conference of the IEEE Engineering in Medicine and Biology Society (EMBC)*, 2018, pp. 878–882.

[11] Q. Duan, E. Angelini, T. Song, and A. Laine, "Fast interpolation algorithms for real-time three-dimensional cardiac ultrasound," in *Proceedings of the 25th Annual International Conference of the IEEE Engineering in Medicine and Biology Society (IEEE Cat. No.03CH37439)*, vol. 2, 2003, pp. 1192–1195 Vol.2.

[12] M. E. Legget, D. F. Leotta, E. L. Bolson, J. A. McDonald, R. W. Martin, X.-N. Li, C. M. Otto, and F. H. Sheehan, "System for quantitative three-dimensional echocardiography of the left ventricle based on a magnetic-field position and orientation sensing system," *IEEE Transactions on Biomedical Engineering*, vol. 45, no. 4, pp. 494–504, 1998.

[13] C. D. Barry, C. P. Allott, N. W. John, P. M. Mellor, P. A. Arundel, D. S. Thomson, and J. C. Waterton, "Three-dimensional freehand ultrasound: Image reconstruction and volume analysis," *Ultrasound in Medicine & Biology*, vol. 23, no. 8, pp. 1209–1224, 1997. [Online]. Available: https://www.sciencedirect.com/science/article/pii/S0301562997001233

[14] R. W. Prager, R. N. Rohling, A. H. Gee, and L. Berman, "Rapid calibration for 3-D freehand ultrasound," *Ultrasound in Medicine & Biology*, vol. 24, no. 6, pp. 855–869, 1998. [Online]. Available: https://www.sciencedirect.com/science/article/pii/S0301562998000441

[15] D. G. Gobbi and T. M. Peters, "Interactive Intra-operative 3D Ultrasound Reconstruction and Visualization BT," in *Medical Image Computing and Computer-Assisted Intervention — MICCAI 2002*, T. Dohi and R. Kikinis, Eds. Berlin, Heidelberg: Springer Berlin Heidelberg, 2002, pp. 156–163.

[16] U. Scheipers, S. Koptenko, R. Remlinger, T. Falco, and M. Lachaine, "3-D ultrasound volume reconstruction using the direct frame interpolation method." *IEEE transactions on ultrasonics, ferroelectrics, and frequency control*, vol. 57, no. 11, pp. 2460–2470, nov 2010.

[17] Q. Huang, Y. Huang, W. Hu, and X. Li, "Bezier Interpolation for 3-D Freehand Ultrasound," *IEEE Transactions on Human-Machine Systems*, vol. 45, pp. 385–392, 2015.

[18] Q. Huang, Z. Yang, W. Hu, L. Jin, G. Wei, and X. Li, "Linear Tracking for 3-D Medical Ultrasound Imaging," *IEEE Transactions on Cybernetics*, vol. 43, no. 6, pp. 1747–1754, 2013.

[19] L. G. Bouchet, S. L. Meeks, G. Goodchild, F. J. Bova, J. M. Buatti, and W. A. Friedman, "Calibration of three-dimensional ultrasound images for image-guided radiation therapy," *Physics in Medicine and Biology*, vol. 46, no. 2, pp. 559–577, 2001. [Online]. Available: http://dx.doi.org/10.1088/0031-9155/46/2/321